Computer simulation of local order in condensed phases of silicon

Frank H. Stillinger and Thomas A. Weber
AT&T Bell Laboratories, Murray Hill, New Jersey 07974
(Received 7 November 1984)

A model potential-energy function comprising both two- and three-atom contributions is proposed to describe interactions in solid and liquid forms of Si. Implications of this potential are then explored by molecular-dynamics computer simulation, using 216 atoms with periodic boundary conditions. Starting with the diamond-structure crystal at low temperature, heating causes spontaneous nucleation and melting. The resulting liquid structurally resembles the real Si melt. By carrying out steepest-descent mappings of system configurations onto potential-energy minima, two main conclusions emerge: (1) a temperature-independent inherent structure underlies the liquid phase, just as for "simple" liquids with only pair interactions; (2) the Lindemann melting criterion for the crystal apparently can be supplemented by a freezing criterion for the liquid, where both involve critical values of appropriately defined mean displacements from potential minima.

I. INTRODUCTION

In contrast to most other elements, the tetrahedral semiconductors Si and Ge shrink when they melt.[1] The crystalline forms of these substances have the open diamond structure with each atom bonded to four others in a tetrahedral pattern. Diffraction experiments[2–4] show that melting causes a partial collapse of this structure whereby coordination number 4 in the crystal increases substantially to an average value exceeding 6. Electrical properties are strongly affected by this profound structural change: Conductivity jumps by a factor of 20 in Si, and of 11 in Ge.[1]

Predicting details of the changes in local order for the tetrahedral semiconductors as they melt provides an irresistible challenge to theory. For the most part, recent theoretical progress in understanding classical liquids and the melting process has concentrated on relatively simple model systems, specifically those with additive pair interactions.[5–7] Liquified noble gases (Ar, Kr, Xe) typify such systems, for which the famous Lennard-Jones (LJ) interaction

$$v_{\mathrm{LJ}}(r)=-4\varepsilon[(\sigma/r)^{12}-(\sigma/r)^{6}] \tag{1.1}$$

constitutes an important paradigm.

Quite obviously, the tetrahedral semiconductors fall in a very different class. No reasonable pair potential will stabilize the diamond structure, as v_{LJ} stabilizes the close-packed crystals characteristic of the noble gases. It is not even clear at the outset that *any* temperature- and density-independent potential could successfully describe liquid semiconductors, since they are not molecular insulators but contain conduction electrons. Nevertheless, the existence of just such a potential (or family of potentials) is an important topic toward which this work has been directed.

In Sec. II we propose a specific nonadditive interaction potential for the condensed phases of Si, and indicate how it was selected. The molecular-dynamics simulation technique used to infer local order and other attributes of the condensed phases that are implied by this potential has been outlined in Sec. III. That outline also includes a discussion of the configurational mapping procedure which we have previously found useful in analyzing the local order that is present in condensed phases.[8–10] In Sec. IV we present some thermodynamic properties displayed by our 216-atom computer simulations, while in Sec. V we provide results concerning local order. In Sec. VI we consider results from the mapping onto potential minima. In Sec. VII we focus briefly on the Lindemann melting criterion,[11] and indicate the possibility that a new "inverse Lindemann criterion" for freezing of liquids can be formulated. In Sec. VIII we assess the overall validity of the present model, and attempt to identify directions for subsequent improvement and applications.

II. NONADDITIVE POTENTIAL

Any potential-energy function Φ describing interactions among N identical particles can quite generally be resolved into one-body, two-body, three-body, etc. contributions as follows:

$$\Phi(1,\ldots,N)=\sum_{i} v_1(i)+\sum_{\substack{i,j\\ i<j}} v_2(i,j)+\sum_{\substack{i,j,k\\ i<j<k}} v_3(i,j,k) +\cdots+v_N(1,\ldots,N)\ . \tag{2.1}$$

In order that this representation be useful in the usual types of theoretical modeling, it is necessary that the component functions v_n converge quickly to zero with increasing n.

The single-particle potential v_1 normally describes wall and external forces to which the system is subject. These are absent for the case considered below, so the expansion (2.1), in principle, begins with the pair-interaction terms.

In view of the fact that the Si crystal consists of atoms held in place by strong and directional bonds, it seems reasonable at first sight that the corresponding Φ could be approximated by a combination of pair and triplet poten-

tials, v_2 and v_3. That will be our point of view in the following. In the same spirit as that behind Eq. (1.1), we first introduce energy and length units ε and σ, and then write

$$v_2(r_{ij})=\varepsilon f_2(r_{ij}/\sigma)\ ,$$
$$v_3(\mathbf{r}_i,\mathbf{r}_j,\mathbf{r}_k)=\varepsilon f_3(\mathbf{r}_i/\sigma,\mathbf{r}_j/\sigma,\mathbf{r}_k/\sigma)\ , \tag{2.2}$$

where ε is chosen to give f_2 depth -1, and σ is chosen to make $f_2(2^{1/6})$ vanish. That f_2 must be a function only of scalar distance is obvious; similarly, f_3 must possess full translational and rotational symmetry.

In the present context, selection of interactions between Si atoms is a considerably more demanding task than that confronted when attempting only to describe small displacements from the ideal tetrahedral geometry. The latter suffices to describe elastic properties and phonon spectra of the crystalline material. In such a restricted regime it may be appropriate to utilize potentials of the Keating type.[12] Now, however, it is mandatory to span the entire available configuration space in order to achieve a satisfactory description of the short-range order in the liquid phase, and of the atom-exchanging diffusive motions that occur continuously in the liquid phase.

The reduced pair potential for use in our study was selected from the following five-parameter family:

$$f_2(r)=\begin{cases}A(Br^{-p}-r^{-q})\exp[(r-a)^{-1}]\ , & r<a\\ 0\ , & r\geq a\end{cases} \tag{2.3}$$

where A, B, p, and a are positive. This generic form automatically cuts off at $r=a$ without discontinuities in any r derivatives, which is a distinct advantage in any molecular-dynamics simulation application.

The same cutoff advantage can be extended to the three-body interactions f_3. Specifically, we assign them the form

$$f_3(\mathbf{r}_i,\mathbf{r}_j,\mathbf{r}_k)=h(r_{ij},r_{ik},\theta_{jik})+h(r_{ji},r_{jk},\theta_{ijk})+h(r_{ki},r_{kj},\theta_{ikj})\ , \tag{2.4}$$

where θ_{jik} is the angle between $\mathbf{r}_j$ and $\mathbf{r}_k$ subtended at vertex i, etc. The function h belongs to a two-parameter family ($\lambda,\gamma>0$). Provided that both r_{ij} and r_{ik} are less than the previously introduced cutoff a, it has the following form:

$$h(r_{ij},r_{ik},\theta_{jik})=\lambda\exp[\gamma(r_{ij}-a)^{-1}+\gamma(r_{ik}-a)^{-1}]\times(\cos\theta_{jik}+\tfrac{1}{3})^2\ ; \tag{2.5}$$

otherwise h vanishes identically. The "ideal" tetrahedral angle θ_t is such that

$$\cos\theta_t=-\tfrac{1}{3}\ , \tag{2.6}$$

so that the trigonometric part of expression (2.5) clearly discriminates in favor of pairs of bonds emanating from vertex i with the desired geometry.

We have carried out a limited search over the seven parameters A, B, p, q, a, λ, and γ to identify a reasonable choice of f_2 and f_3. An important component of this search was an evaluation of lattice sums to ensure that the diamond structure was indeed the most stable periodic arrangement of particles at low pressure, at least among simple alternatives. However, after this lattice-sum criterion was satisfied, it was still necessary that the melting point and the liquid structure inferred for the tentative interaction by the molecular-dynamics simulation also be in reasonable accord with experiment. These latter criteria served to contribute to our rejection of several of our initial choices for parameter sets.

Overall, the most satisfactory parameter set thus far discovered is the following:

$$A=7.049\,556\,277\ ,\quad B=0.602\,224\,558\,4\ ,$$
$$p=4\ ,\quad q=0\ ,\quad a=1.80\ , \tag{2.7}$$
$$\lambda=21.0\ ,\quad \gamma=1.20\ .$$

This is the choice upon which all results reported in the remainder of this paper are based.

Figure 1 shows the corresponding binding energy per atom Φ/N (in reduced units) versus number density ρ (also in reduced units) for several simple lattices. Although at zero pressure the diamond structure (DIA) is preferred, the other cases—simple cubic (sc), body-centered cubic (bcc), and face-centered cubic (fcc)—are reasonably close. We believe that this closeness is important in assuring that thermodynamic melting to a collapsed liquid structure be possible at a reasonable temperature. By construction, the sum of three-body interactions nearly vanishes for the diamond structure. Although that sum substantially destabilizes the other lattices, these alternative structures partially compensate by incorporating more of the stabilizing pair bonds than does the diamond lattice. Evidently, it is important to achieve a proper balance between these competing effects in order to model Si successfully.

At the minimum in the diamond curve of Fig. 1,

$$\rho=0.460\sigma^{-3}\ ,\quad \Phi/N=-1.999\,993\varepsilon\ . \tag{2.8}$$

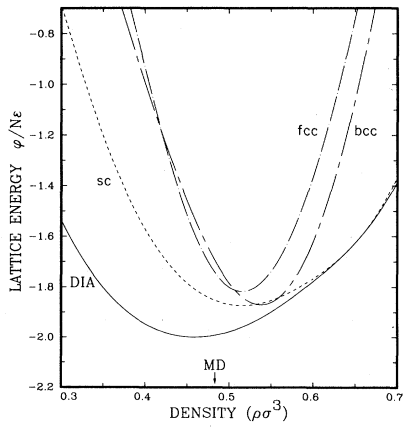

FIG. 1. Lattice energy (per atom) vs density for the nonadditive Si potential. Equation (2.7) provides the parameter set used for the interactions. The arrow locates the density at which our molecular-dynamics calculations were performed. (See text for label legend.)

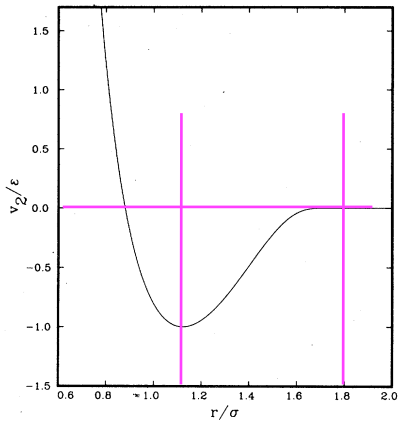

FIG. 2. Reduced pair potential vs distance. This function vanishes identically beyond $r=1.80$.

In order for these to correspond to the observed lattice spacing and atomization energy of crystalline Si at 0 K, it would be necessary to choose

$$\begin{aligned}&\sigma=0.209\,51\ \text{nm}\ ,\\ &\varepsilon=50\ \text{kcal/mol}\\ &\quad=3.4723\times10^{-12}\ \text{erg/at. pair}\ .\end{aligned}\tag{2.9}$$

Figure 2 shows the reduced pair potential f_2 as a function of reduced distance.

III. MOLECULAR-DYNAMICS SIMULATION

Our computer simulation has utilized $N=216$ atoms in a cubic cell with fixed volume. Periodic boundary conditions were applied at all six faces of the cell. Because primary interest concerned the liquid phase, we elected to keep the mass density equal to that of the real liquid at its observed melting point, 1410 °C, namely 2.53 g/cm^3.[1] The mass of the common stable isotope ^{28}Si is

$$m=4.6457\times10^{-23}\ \text{g/at.}\ ,\tag{3.1}$$

so that the edge length of the cubic cell must be given the value

$$L=7.646\,14\sigma=1.605\,31\ \text{nm}\ .\tag{3.2}$$

The corresponding number density for the 216 atoms,

$$\rho=0.4832\sigma^{-3}\ ,\tag{3.3}$$

exceeds that shown in Eq. (2.8) for the zero-pressure, zero-temperature crystal. The integer $N=216$ has just the proper form to permit the atoms to be arranged in a defect-free diamond lattice, aligned with the sides of the cubic cell, while bonding perfectly across its faces to periodic-image atoms. The lattice sum for this somewhat compressed crystal is

$$\Phi/N=-1.992\,346\varepsilon\ .\tag{3.4}$$

The molecular-dynamics study for the model was initiated with the 216 atoms placed in the compressed crystalline arrangement, with a random set of very small momenta. The given two- and three-body potentials in Φ lead to explicit force expressions for each particle which enter the Newtonian equations of motion. The latter were integrated using a fifth-order Gear algorithm,[13] and incremental time step $\Delta t=5\times10^{-3}\tau$, where the basic time unit is

$$\tau=\sigma(m/\varepsilon)^{1/2}=7.6634\times10^{-14}\ \text{s}\ .\tag{3.5}$$

Under these circumstances the total energy would remain constant to at least seven significant figures during runs typically of several thousand Δt. Temperature was adjusted by the usual method of scaling all momenta by a common factor.

During some of the molecular-dynamics runs to be discussed below, the instantaneous atom configuration $\mathbf{r}_1(t),\ldots,\mathbf{r}_N(t)$ was periodically mapped onto the configuration $\mathbf{r}_{1q},\ldots,\mathbf{r}_{Nq}$ of a nearby Φ minimum. In no sense did this mapping disturb the system's Newtonian dynamics; it was simply a computation carried out in parallel. The mapping was accomplished by using Newton's method to find the limiting ($s\to\infty$) solution to the steepest-descent equations,

$$\frac{d\mathbf{r}_j}{ds}=-\nabla_j\Phi\ ,\tag{3.6}$$

where the dynamical configuration supplies the initial condition. In principle, then, any instantaneous set of atom positions can be uniquely referred to a mechanically stable structure. Determining what the available Φ minima are for the Si model, and how they are serially sampled at different temperature, constituted one of the important goals for this project.

IV. THERMODYNAMIC PROPERTIES

Figure 3 presents some of our molecular-dynamics data for the mean potential energy per particle,

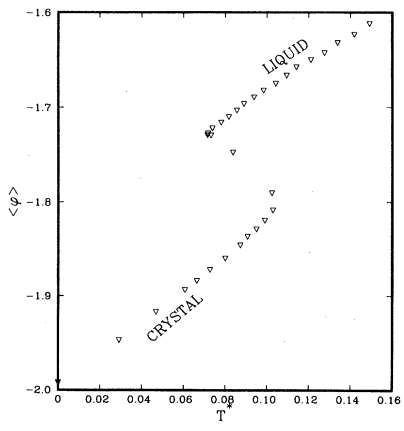

FIG. 3. Mean potential energy per particle vs temperature for the Si model. The points shown represent a sequence of molecular-dynamics runs during which the total system energy was systematically increased from case to case (with equilibration).

$$\langle\varphi\rangle=\langle\Phi\rangle/N\varepsilon\ , \tag{4.1}$$

versus reduced temperature,

$$T^*\equiv k_BT/\varepsilon\ . \tag{4.2}$$

The positive temperature points shown in the figure emerge from a sequence of molecular-dynamics runs (each preceded by its own equilibration run), between pairs of which the total energy was monotonically increased. The perfect crystal at absolute zero provided the starting point. Runs were subsequently generated by giving atoms very small random momenta, and then by sequentially scaling up the momenta between runs by an appropriate factor greater than unity. After each scaling an equilibration period was permitted to run 500 time steps followed by a subsequent averaging period for 1500 steps, while the system was obviously still in its crystalline phase (lower branch in Fig. 3). For the remainder of the sequence, which included melting and heating of the resulting liquid, the equilibration and averaging periods were 1000 and 3000 steps, respectively.

The retrograde behavior displayed in Fig. 3 is characteristic of a first-order phase change. The existence of a positive latent heat implies that the temperature will drop when melting occurs at constant total energy, or, as in the present circumstance, even when the total energy is slowly increased.

The liquid branch of the $\langle\varphi\rangle$-versus-T^* curve has been reproduced during stepwise reduction in total system energy, and for that reason we believe the results shown in Fig. 3 are a correct reflection of thermal equilibrium in our small system. The crystal branch is probably reliable as well since it agrees accurately below the melting region with the expected equipartition result for harmonic normal modes. We have not attempted to recreate that crystal branch by cooling the liquid until it spontaneously froze.

No doubt the upper limit of stability for the crystal shown in Fig. 3 at $T^*\cong 0.103$ represents an effective limit of superheating. The crystal contained no surfaces or inserted defect sites at which melting could easily initiate. Therefore, the thermodynamic melting temperature must be somewhat lower. We estimate it to be

$$T_m^*\cong 0.080\ . \tag{4.3}$$

At this temperature the difference in $\langle\varphi\rangle$ between the liquid and crystal branches is

$$\langle\varphi\rangle_l-\langle\varphi\rangle_c=0.295\ . \tag{4.4}$$

Consequently, the entropy change that would accompany reversible transfer of the system from crystal to liquid would be

$$\Delta S/Nk_B\cong 3.7\ . \tag{4.5}$$

This constant-volume, constant-temperature result can be compared with the constant-pressure experimental melting value at 1 atm:[14]

$$\Delta S(\text{expt})/k_B=3.25\ . \tag{4.6}$$

In comparing these numbers, it is important to keep in mind that the molecular-dynamics crystal is under substantial compression.

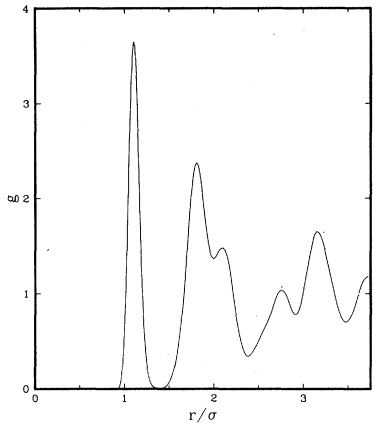

FIG. 4. Pair-correlation function for the Si model in the crystal phase at $T^*=0.0800$.

The equipartition value of $C_v^*\equiv C_v/Nk_B\varepsilon$, the reduced constant-volume heat capacity that is relevant to the low-temperature crystal, is equal to

$$C_v^*=\tfrac{3}{2}\ . \tag{4.7}$$

At T_m^* this has been observed to rise to

$$C_v^*(T_m^*,\text{cryst})\cong 2.0 \tag{4.8}$$

as a result of anharmonicity in the lattice. The corresponding result for the liquid at T_m^* is found to be

$$C_v^*(T_m^*,\text{liq})\cong 1.6\ ; \tag{4.9}$$

furthermore, this quantity in the liquid tends to diminish as T^* rises.

V. LOCAL ORDER

The pair-correlation function $g(r)$ offers a convenient way to observe and analyze local order in condensed sys-

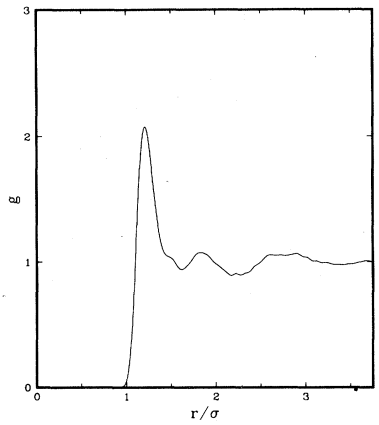

FIG. 5. Pair-correlation function for the Si model in the liquid phase at $T^*=0.0817$.

tems.[5–7] This function is defined to be proportional to the mean number of atom pairs with vector separation $\mathbf{r}$, averaged over all directions of $\mathbf{r}$, with normalization to unity for a random distribution of atoms.

Figures 4 and 5, respectively, show $g(r)$ extracted from crystal- and liquid-phase molecular-dynamics runs near T_m^*. The first of these is highly structured, revealing the organization of atoms into well-defined coordination shells. Running coordination numbers $n(r)$ may be obtained from $g(r)$ as follows:

$$n(r)=4\pi\rho\int_0^r s^2 g(s)ds\ , \tag{5.1}$$

and, as expected, this yields four nearest neighbors when it is evaluated at the deep minimum in Fig. 4 beyond the fully resolved first peak. Although second- and higher-order coordination shells in Fig. 4 run into each other somewhat, their positions and magnitudes are just as expected for a vibrating but structurally perfect diamond lattice. Corresponding g results for the crystal at lower temperature show greater coordination-shell resolution.

Comparison of the liquid-phase g with that for the crystal provides stark testimony to the profound structural breakdown that occurs at melting. With the exception of a broader and considerably lower first peak, coordination-shell structure, as such, has become very indistinct. In particular, the gap appearing in Fig. 4 between the first and second coordination shells for the crystal has disappeared. A broad and weak second maximum is present in the liquid-phase g spanning the range between 1.35 and 1.80 times the distance to the first maximum, which is consistent with some minor persistence of tetrahedral bonding into the liquid. The running coordination number $n(r)$ is equal to 8.07 at $r/\sigma=1.625$, the position of the shallow first minimum in Fig. 5.

It is useful to examine the structure factor $S(k)$ corresponding to a given $g(r)$, on account of its relation to diffraction experiments and to density fluctuations in the medium at wave vector $\mathbf{k}$. We have, for a liquid,

$$S(k)=N^{-1}\sum_{j,l=1}^{N}\langle\exp[i\mathbf{k}\cdot(\mathbf{r}_l-\mathbf{r}_j)]\rangle$$
$$=1+\rho\int\exp(i\mathbf{k}\cdot\mathbf{r})[g(r)-1]d\mathbf{r}\ . \tag{5.2}$$

Figure 6 shows $S(k)$ for the same liquid state at $T^*=0.0817$. On account of finite-system truncation errors, the curve shown is inaccurate for $k\sigma<2.5$; however, the remainder of the curve is significant. The most notable feature is the first maximum at $k\sigma=5.3$ with an obvious shoulder at $k\sigma=6.8$. This pattern always appears when the liquid is near T_m^*. The subsequent maxima shown in Fig. 6 with diminishing amplitudes occur at $k\sigma=11.2$, 17.1, and 22.2.

When the present results are compared with those from diffraction experiments[2,3] on molten Si, the conclusion seems to be that our model is qualitatively successful in describing local order in the liquid, although moderate quantitative discrepancies appear. Specifically, the shouldered first peak in $S(k)$ is a very prominent feature in the experimental results, followed by relatively unstructured subsequent peaks with diminishing amplitudes. Furthermore, this $S(k)$ pattern, experimentally, is only observed for molten Si and Ge among all elemental substances. By using the σ value in Eq. (2.9) to express our molecular-dynamics results in more familiar units, it can be verified that peak and shoulder positions agree satisfactorily with experiment. The comparison is given in Table I.

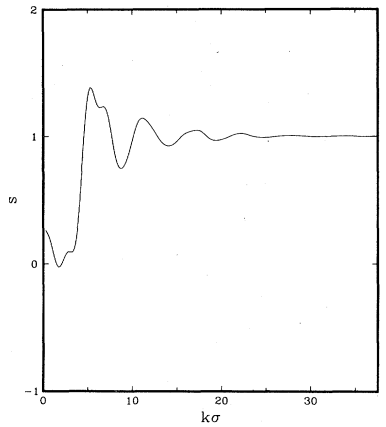

FIG. 6. Structure factor for the liquid-Si model at $T^*=0.0817$.

Not surprisingly, the direct-space comparison of pair-correlation functions is also qualitatively satisfactory. The molecular-dynamics (MD) function displayed in Fig. 5 has its first maximum at $r_1=0.256$ nm, with

$$g(r_1)=2.06\ \ (\text{MD})\ ; \tag{5.3}$$

experimentally,[3] $r_1=0.250$ nm and

$$g(r_1)=2.23\ \ (\text{expt}) \tag{5.4}$$

at 1430°C. In addition, the relatively flat behavior observed for $g(r)$ in the present calculations beyond the first peak also appears in the experimental results. We refer the reader to figures appearing in Refs. 2 and 3 for specific details.

The "mean number of nearest neighbors" in liquid Si experimentally has been reported as 6.4 both by Waseda and Suzuki[2] and by Gabathuler and Steeb.[3] However, in neither reference was the precise definition of that quantity given, nor were limits of uncertainty stated. Conse-

TABLE I. Comparison of structure-factor positions in k space. (Units for k are Å^{-1}.)

Feature[a]	Molecular dynamics[b]	Experiment[c]
First peak	2.53	2.80
Shoulder	3.25	3.25
Second peak	5.35	5.75
Third peak	8.16	8.50
Fourth peak	10.60	11.20

[a]Refer to Fig. 6.
[b]For $T^*=0.0817$.
[c]From Waseda and Suzuki, Ref. 2, Fig. 1, for liquid Si at 1460°C.

quently, it is not entirely clear whether our own result for $n(r)$ at the first $g(r)$ minimum, namely 8.07, is in fact too large. In any case both experiment and the molecular-dynamics simulation agree that the "mean number of nearest neighbors" in liquid Si is substantially less than in other elemental liquids (typically, 10—12).

VI. MAPPING TO POTENTIAL MINIMA

Previous applications[8–10] have shown that mapping of system configurations onto nearby potential-energy minima illuminates the nature of short-range order present in condensed phases. Furthermore, this technique is useful in suggesting the form that should be adopted by analytical theory of the solid-liquid transition.[15,16]

Numerically solving the steepest-descent equation (3.6) to locate the relevant minimum for any given initial configuration is a demanding task for the specific 216-atom system under consideration. Nevertheless, we have done such calculations for a few selected circumstances that seemed to warrant the effort.

One of the principal results that has emerged from earlier mapping studies has been that a virtually temperature-independent inherent structure underlies the liquid state. While it is true that the pair-correlation functions $g(r,T)$ are typically and clearly temperature dependent (at constant density), the corresponding functions $g_q(r)$ evaluated for the sets of mapped configurations from each state are not. That is, the temperature dependence observed for pair correlation in those simple liquids thus far examined consists entirely of variation in "vibrational" displacement away from potential minima, and not in substantial population shifts among regions belonging to distinct groups of minima. The models for which this phenomenon has been previously verified all involve additive central potentials between the constituent particles. It is important now to see whether the strong nonadditivity operative in the present model for Si affects that phenomenon.

Figure 7 shows the "inherent" pair-correlation function

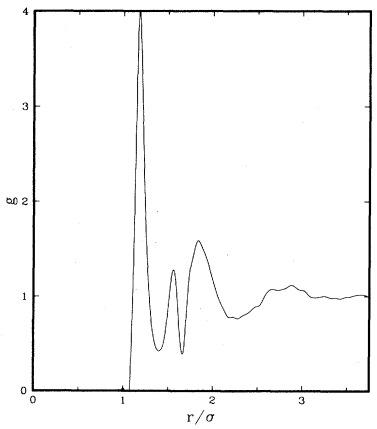

FIG. 7. "Inherent" pair-correlation function for liquid Si. The temperature in the slightly supercooled melt from which the 31 contributing potential minima were constructed was $T^*=0.0677$.

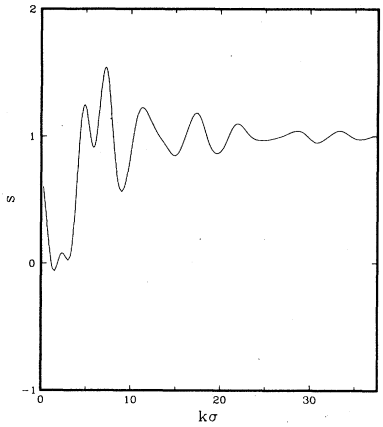

FIG. 8. Structure factor corresponding to the "inherent" pair-correlation function of Fig. 7. The $k\sigma<2.5$ regime contains substantial truncation error and should be disregarded.

$g_q(r)$ obtained from a molecular-dynamics run on slightly supercooled molten Si at $T^*=0.0677$. Figure 8 provides the corresponding structure factor. These results are based on atom configurations for 31 potential-energy minima which were obtained from molecular-dynamics configurations separated by $100\Delta t$. The distribution of Φ values at these minima appears to be sufficiently irregular to suggest that comprehensive and representative configuration-space sampling has occurred.

The conventional pair-correlation function $g(r)$ for this supercooled liquid closely resembles that shown in Fig. 5. However, the mapping onto minima has produced a dramatic degree of structural enhancement, as might have been expected. Nevertheless, the sharp features exhibited by $g_q(r)$ clearly are not those of the crystalline solid, as comparison with Fig. 4 readily reveals.

Figure 9 shows the conventional pair-correlation function $g(r)$ for a very hot fluid at $T^*=0.1492$. Not surprisingly, this function possesses substantially less short-range order than that for the cooler liquid (at $T^*=0.0817$) in

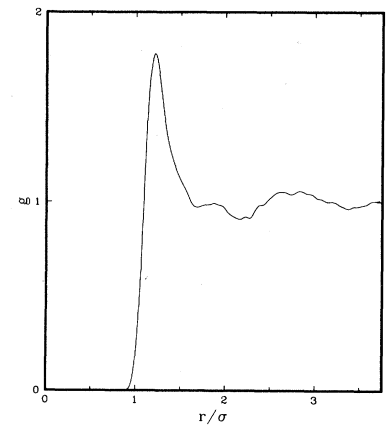

FIG. 9. Conventional pair-correlation function for hot molten Si at $T^*=0.1492$.

Fig. 5. Figure 10 shows the corresponding "inherent" pair-correlation function $g_q(r)$. The latter represents an average over 30 configurations at Φ minima, where the initial configurations along the dynamical trajectory were separated by $100\Delta t$ as before.

The two g_q's in Figs. 7 and 10 must be regarded as essentially identical. Differences between the curves are very small everywhere, and, in any case, are of the order of statistical errors associated with our necessarily restricted sampling. Once again we conclude that temperature variations observed for $g(r,T)$ at constant density arise strictly from amplitude variation of "vibrational" motion within regions surrounding minima, and not from a shifting equilibrium between such regions.

Running coordination numbers n_q can be calculated for g_q using Eq. (5.1). On this basis we find, for the nearly identical g_q's in Figs. 7 and 10, that n_q is 4.80 at the first minimum beyond the sharp first peak of g_q, and rises to 7.95 at the second minimum. This increment of just over three atoms occurs at a smaller distance than do second neighbors in the diamond lattice, and appears to be associated with the end-to-end distances of nearly-right-angled arrangements of atom triads.

Although the mechanically stable atom arrangements which contribute to the $g_q(r)$ are amorphous Si deposits, one must avoid the temptation to identify them with real amorphous Si formed by various means in the laboratory. These latter materials doubtless vary in properties with method of preparation, and may have enjoyed the opportunity to engage in localized partial crystallization.

The rather deep first minimum at $r/\sigma=1.40$ in the common g_q function suggests using this distance as a cutoff criterion for examination of bonding statistics. Thus any pair of atoms in a mechanically stable packing (Φ minimum) whose separation is less than this cutoff will be counted as bonded, while any pair with greater distance will not. Obviously, alternative definitions are possible, in particular, using the strengths of interaction between atoms. In any event, our simple geometrical criterion agrees with the known structure of the diamond lattice, with all nearest neighbors counted as bonded and no others.

TABLE II. Fractions of Si atoms with various numbers of bonds in the collections of potential minima which define liquid-phase "inherent structure."

Number of bonds[a]	Fraction of atoms
2	0.000
3	0.000
4	0.201
5	0.568
6	0.205
7	0.024
8	0.001
9	0.000

[a]The bond count utilizes $r/\sigma=1.40$ as an upper cutoff criterion.

In Table II we present the fractions of Si atoms found, with this cutoff criterion, to engage in various numbers of bonds in the collection of Φ minima that define inherent structure for the liquid. Four-coordinate atoms are still present, but they are dominated by five-coordinate atoms, and higher coordination numbers frequently appear as well. Note, however, that the angle-dependent three-body interactions prevent any occurrence of coordination numbers near 12 that would indicate local close packing.

VII. MELTING AND FREEZING CRITERIA

Prior experience indicates how mapping of dynamical-path configurations onto potential-energy minima can be a particularly useful tool for studying melting and freezing.[16] Consequently, we have applied this technique to a dynamical sequence during which a somewhat superheated Si crystal spontaneously underwent nucleation and melting to produce homogeneous liquid.

In Fig. 11 we present values of Φ/N at the minima which were attained by the steepest-descent mapping. As before, the elapsed time between successive mappings was $100\Delta t$. At the initial sampling step (labeled 0 in Fig. 11) the steepest descent brought the system to one of the absolute minima corresponding to a structurally perfect dia-

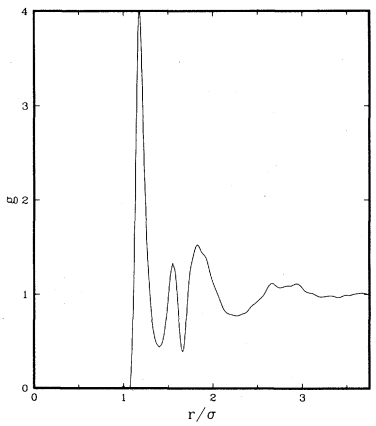

FIG. 10. "Inherent" pair-correlation function for hot molten Si at $T^*=0.1492$.

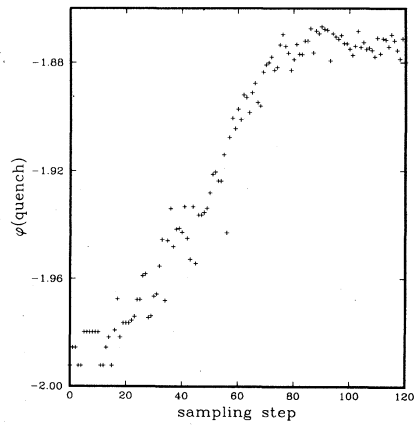

FIG. 11. Values of potential energy per particle at minima attained by periodic mapping during melting.

mond lattice. At this, and roughly the following 15 mappings, the system was recognizably crystalline, with a temperature $T^* \cong 0.102$. That the absolute minimum was not encountered every time during this unmelted "first stage" reflects the strongly anharmonic character of the superheated crystal: Thermal fluctuations cause localized defects spontaneously to form and to annihilate.

After this first stage, nucleation of the liquid occurred, and the depths of the potential-energy minima produced by the mapping drifted upward, as Fig. 11 clearly demonstrates. Judging by the pair-correlation functions and the distributions of intact bonds as defined above, liquid and crystal coexist throughout this stage with the former increasing in extent at the expense of the latter.

The second stage, melting, terminates at about mapping step 80. Subsequently, the depths of the potential minima show no further upward drift, but fluctuate narrowly about a mean value

$$\langle \Phi_q \rangle / N \cong -1.873 \ . \tag{7.1}$$

In this third stage the system is homogeneously liquid, at $T^* \cong 0.0677$, and is therefore somewhat undercooled. The distribution of potential-energy minima sampled by this relatively cold liquid is substantially the same as that sampled by much hotter liquids at the same density, and this fact underlies the existence of a temperature-independent inherent structure.

The mapping operation moves all atoms in a systematic way until they are simultaneously subject to no force. It is illuminating to inquire how large on the average these atom displacements are required to be. For any given dynamical configuration $\mathbf{r}_1, \ldots, \mathbf{r}_N$ and its mapping $\mathbf{r}_{1q}, \ldots, \mathbf{r}_{Nq}$, we can evaluate, for example,

$$\langle r \rangle = N^{-1} \sum_{j=1}^{N} | \mathbf{r}_j - \mathbf{r}_{jq} | \ . \tag{7.2}$$

Figure 12 shows these mean scalar displacements for return to potential minima for each of the same 121 mappings upon which Fig. 11 was based. This shows not only the behavior in the superheated crystal, but the dramatic effect of melting.

The mean mapping distance in a low-temperature crystal would be determined by the amplitudes of harmonic phonon motions that are present, and classically should scale as $(T^*)^{1/2}$. As the temperature rises toward the melting point, anharmonic processes could be expected to increase the mean distance slightly, but it should still behave qualitatively as in the harmonic regime. The Lindemann melting criterion[11] specifies that melting occurs when the root-mean-square displacement of atoms reaches a critical fraction of the lattice spacing, typically about $\frac{1}{7}$.[17,18] At the present level of precision it is unnecessary to distinguish rms averages from the average defined in Eq. (7.2) above. The stage-1 mean distances shown in Fig. 12 average approximately 0.19 times the lattice spacing in the static crystal, and considering the fact that the solid is a bit superheated, this is consistent with Lindemann-law expectations.

After melting, the mean mapping distances presented in stage 3 of Fig. 12 are approximately 0.29 times the

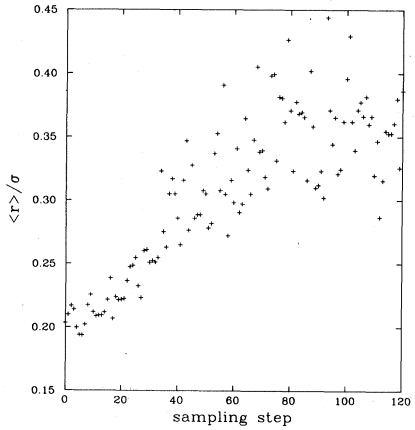

FIG. 12. Mean distances of atom displacement under the mappings utilized in Fig. 11.

nearest-neighbor separation (defined in the liquid as the distance to the first maximum of g, about 10% larger than the lattice spacing). Furthermore, the mean mapping distances from one case to the next display considerably greater relative dispersion than those in stage 1 for the unmelted solid. These greater distances and dispersions may provide valuable geometric information about the multidimensional mapping regions encountered in the liquid phase.

Just as in the situation for the crystal, raising the temperature in the liquid causes the mean mapping distances for the atoms to increase. At $T^* = 0.1492$ they have risen to 0.39 times the nearest-neighbor separation.

These observations generate an intriguing possibility, namely that a freezing criterion for liquids might theoretically exist as a complement to the Lindemann melting criterion for solids. Present evidence seems to suggest that when cooling the liquid causes the mean atomic mapping distance to drop to about three-tenths of the neighbor spacing, freezing occurs. The introduction of the steepest-descent mapping operation, applicable to any phase of matter, is the key needed to effect extension of the simple and appealing Lindemann criterion to liquids, where, conventionally, its concepts would have been thought to be totally inapplicable.

Nucleation for the melting process apparently requires proliferation and aggregation of defects in the anharmonic crystalline medium. Mapping onto potential-energy minima is a valuable tool for studying how this occurs.[16] One of the basic questions here concerns the nature of the separate defects that spontaneously form under thermal agitation in the solid. By examining the structures and energies for those minima lying just above the absolute minimum, it should be possible to answer this question.

The lowest-lying minimum above the absolute minimum, which was encountered during the stage-1 sampling in Figs. 11 and 12, appeared at sampling step 13. Its structural excitation energy relative to the perfect-crystal absolute minimum was found to be $1.445\,81\varepsilon$. For any geometric definition of bonding with a cutoff in the range

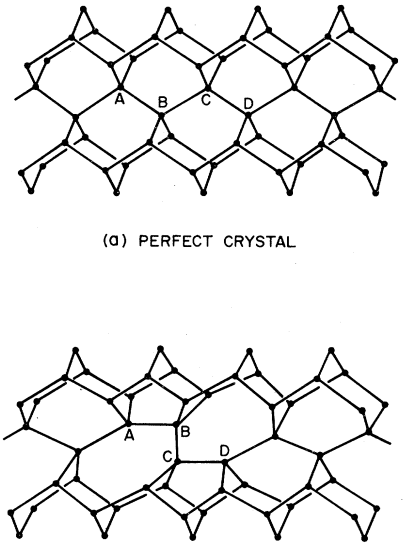

FIG. 13. Rebonding scheme in formation of a localized topological defect in the Si crystal.

$$1.15 \leq r_c/\sigma \leq 1.45 \tag{7.3}$$

(which includes the choice used earlier), every one of the 216 Si atoms participates in exactly four bonds in this defect-containing structure. Consequently, the defect must entail some kind of topological reconnection of the bonds in the crystal.

In the defect-free Si crystal the bonds are arranged so that all closed paths along successive bonds are polygons with an even numbers of sides (6, 8, 10,...). Our examination of stereo pictures for the defect configuration under consideration shows that odd polygons have been introduced at the defect, specifically including pentagons and heptagons. The rebonding scheme is shown in Figs. 13(a) and 13(b). By construction, this is a locally strained but mechanically stable arrangement of Si atoms. We are presently unable to say if such a topological defect would be an important entity in real Si, but further study of this possibility seems to be warranted.

VIII. DISCUSSION

The silicon model examined in this paper seems to be qualitatively successful in representing condensed phases of that substance, but it clearly has quantitative deficiencies. Since its potential-energy function is based on a very limited search, there is good reason to believe that significant improvements are possible.

One of the quantitative problems raised by the present version is that of energy scale. In order for the observed transition temperature, Eq. (4.3), to correspond to the freezing temperature for liquid Si (1410 °C), it is necessary for the basic energy parameter to have the value

$$\varepsilon \cong 42 \text{ kcal/mol} , \tag{8.1}$$

which is considerably less than the 50 kcal/mol needed to provide the correct cohesive energy of the crystal, Eq. (2.9). Although it is possible that changes in v_2 and v_3 might bring T_m^* down sufficiently far to eliminate the discrepancy, another option exists. This option involves augmenting the potential with position-independent single-particle terms v_1 [see Eq. (2.1)], the source of which can be argued to lie in the electronic structure of the material. For the case considered here, we would have to have

$$v_1 \cong -16 \text{ kcal/mol} \tag{8.2}$$

to explain the cohesive energy of the crystal. We would expect v_1 to have some density variation, and therefore to influence compressibility. In any case, addition of v_1 terms to the potential only affects the temperature scale, but has no influence on the local structure that obtains at a given reduced temperature.

Many of the same considerations that relate to selection of a model Si potential are applicable as well to Ge. Their distinct melting temperatures require different energy and temperature scaling factors, of course, but also more subtle distinctions must be observed. Measured pair-correlation functions for the respective liquids at corresponding temperatures show small but significant differences.[2,3] It will be important eventually to see if the general type of molecular-dynamics modeling advocated here can reproduce those differences.

[1]V. M. Glazov, S. N. Chizhevskaya, and N. N. Glagoleva, *Liquid Semiconductors* (Plenum, New York, 1969), Chap. 3.
[2]Y. Waseda and K. Suzuki, Z. Phys. B **20**, 339 (1975).
[3]J. P. Gabathuler and S. Steeb, Z. Naturforsch. **34a**, 1314 (1979).
[4]M. Davidovic, M. Stojic, and Dj. Jovic, J. Phys. C **16**, 2053 (1983).
[5]S. A. Rice and P. Gray, *The Statistical Mechanics of Simple Liquids* (Wiley-Interscience, New York, 1965).
[6]C. A. Croxton, *Liquid State Physics—A Statistical Mechanical Introduction* (Cambridge University Press, London, 1974).
[7]J. P. Hansen and J. R. McDonald, *Theory of Simple Liquids* (Academic, New York, 1976).
[8]F. H. Stillinger and T. A. Weber, Phys. Rev. A **28**, 2408 (1983).
[9]F. H. Stillinger and T. A. Weber, J. Phys. Chem. **87**, 2833 (1983).
[10]F. H. Stillinger and T. A. Weber, J. Chem. Phys. **80**, 4434 (1984).
[11]F. A. Lindemann, Phys. Z. **11**, 609 (1910).
[12]P. N. Keating, Phys. Rev. **145**, 637 (1966).
[13]C. W. Gear, Argonne National Laboratory Report No. ANL-7126 (unpublished).

[14]A. R. Ubbelohde, *The Molten State of Matter* (Wiley, New York, 1978), p 239.
[15]T. A. Weber and F. H. Stillinger, J. Chem. Phys. **81**, 5089 (1984).
[16]F. H. Stillinger and T. A. Weber, J. Chem. Phys. **81**, 5095 (1984).
[17]*Theory of Simple Liquids,* Ref. 7, p. 361.
[18]K. Ishizaki, I. L. Spain, and P. Bolsaitis, J. Chem. Phys. **63**, 1401 (1975).